Journal of Materials Science & Surface Engineering, 7(1): 913-918
ISSN (Online): 2348-8956; 10.jmsse/2348-8956/7-1.2

Study of Microstructure and Wear Behaviour of Duplex Stainless Steel Hardfacing Deposits on Ferritic Ductile Iron Substrate

M. Hajian Foroushani · M.Shamanian · M. Farghadani

Department of Materials Engineering, Isfahan University of Technology, Isfahan, 8415683111, Iran.

ABSTRACT

In this study, cladding of ferritic ductile iron (DI) was performed using duplex stainless steel wire (25.10.4.L) and gas tungsten arc welding (GTAW). The microstructure and wear behaviour of the clad layer and interface were investigated by optical microscope(OM), scanning electron microscope(SEM) and X-ray diffraction analysis. The results showed that the clad layer had a dendritic structure including austenite, ferrite, carbides and nitrides. Also, the results revealed that the preheating temperature was high enough to prevent the formation of brittle martensite phase in the heat affected zone(HAZ). Wear resistance of the clad layer was much higher than that of base metal (BM), possibly due to the presence of the dendritic structure and many carbides and nitrides. In order to understand the wear life of the coated sample, wear test on interface was performed. The wear resistance of interface was significantly higher than that of the clad layer.

ARTICLE HISTORY
Received 07-01-2019
Revised 15-09-2020
Accepted 09-10-2020
Published 20-03-2020

KEYWORDS
Ferritic Ductile Iron
Cladding
Duplex Stainless Steel
Wear

Introduction

Ductile irons (DI) with the nodular graphite structure were developed around 65 years ago [1]. Due to the low production costs, high ductility, good corrosion resistance, good castability and machinability, high absorption of the vibration, high mechanical properties and good fatigue resistance, the ferritic DIs are widely used in the automotive industry as hydraulic pump components (i.e., pistons, pump housing),gear boxes, railway wheels, valves and agricultural machine parts [2-3]. However, under severe conditions, the wear resistance of the ferritic DI is significantly reduced [4]. The wear behaviour of engineering materials depends on the surface features such as surface roughness, surface microstructure and surface hardness. So the wear behaviour of DI can be improved by enhancing these properties in the surface of the materials[4]. Surface modification and surface alloying are two methods used for the modification of the surface properties of materials [5]. Surface alloying process includes many techniques such as cladding. Cladding is defined as the deposit of a dissimilar weld metal laid on the surface of another metal [6]. Recently, cladding process has been used in various industries such as chemical, nuclear and steam power plants, food processing and petrochemical industries[6]. Weld cladding can be carried out by any one of the welding processes such as gas metal arc welding (GMAW), shielded metal arc welding (SMAW), electroslag welding (ESW), plasma arc welding (PAW), flux cored arc welding (FCAW) and gas tungsten arc welding (GTAW) [6, 7]. High deposition rate, high maneuverability, large scale availability, low cost and compatibility with a wide range of materials, precise control, and the high quality of weld metals are some advantages of the GTAW process [7-10]. Numerous materials such as nickel and cobalt alloys, copper alloys, manganese alloys, alloy steels, ceramics, composites, chromium, titanium, vanadium and molybdenum are used for cladding applications; among them, iron alloys with a considerable amount of chromium have attracted more attention than others [6, 8, 11]. Shamanian et al.[11] studied the effect of the coating thickness on the wear behaviour of DI surface modified by austenitic stainless steel. They found that the sample with a thin coating had higher hardness and better wear resistance than the thick coating specimen. The high hardness value of the thin coating specimen was related to hard carbide phases formed in the vicinity of the surface of this sample. In contrast, the microstructure of thick coating specimen only included austenite (Fe,C) and there were no carbide phases. The wear behaviour and the microstructure of nickel base electrode deposited on DI with single and double passes through the SMAW process were investigated by Arabi et al. [12]. They found that the hardness of samples with the single pass coating was higher than that of samples with the double pass coating. The wear resistance was significantly improved in the coated samples (single and double passes). The higher wear resistance of the clad samples, in comparison with that of DI, was related to the presence of hard phases such as iron-chromium carbide and the small amount of martensite. Apart from that, it has been found recently that the wear resistance of DI can be improved by using different materials such as Stellite 6 [13], Inconel 617 [10], molybdenum and chromium powders [14] and C-B-W-Cr powder [15]. However, to the best of authors' knowledge, there seems to be no information regarding the cladding of duplex stainless steel on the surface of ferritic DI in the literature. Duplex ferritic-austenitic stainless steels are defined as a family of steels having a two-phase microstructure with approximately equal volume fractions of austenite and ferrite [16, 17]. Duplex stainless steels enjoy very good mechanical properties and corrosion resistance because of simultaneously having ferrite and austenite phases [17]. Above all, the thermal expansion of duplex stainless steels is close to that of carbon steel, low

Corresponding Author: M. Hajian Foroushani, Tel: +989133700411
Email: mohsen.hajian@ma.iut.ac.ir

Contents lists available at http://www.jmsse.in/ & http://www.jmsse.org/

Table 1: Chemical composition of the filler wire, substrate, the counterpart and the clad layer (wt-%)

Element	Fe	Ni	Cr	Mn	Si	C	N	Mo	P	S
Filler	Bal.	9.5	25	0.4	0.3	≤0.02	0.21	4	≤0.02	≤0.02
Substrate	Bal.	0.5	0.09	0.59	4.18	2.8	-	-	≤0.018	0.05
Pin52100	Bal.	-	1.3-1.6	0.25-0.45	0.15-0.35	0.98-1.1	-	-	≤0.025	≤0.025
Clad layer	Bal.	7.26	19.53	0.42	1.02	0.63	0.15	3/19	≤0.025	≤0.025

alloy steel and cast iron [16]. Thus, these alloys are serious candidates for the cladding of DI. So the aim of the present study was to investigate the microstructure, wear behaviour and hardness of the clad layer of duplex stainless steel deposited on ferritic DI.

Experimental

The specimens with the dimensions of 120 mm × 15 mm × 12 mm were cut from the rectangular bulk of ferritic ductile iron as BM. Duplex stainless steel wire (25.10.4.L), 2.5 mm in diameter and 1000 mm in length, was selected as the coating material. The chemical composition of the filler wire and DI substrate is shown in Table 1. Prior to welding, the sample was cleaned by acetone to remove all contaminations. Then the sample was preheated at 250 ˚C to prevent the formation of any cracking in the BM and HAZ [8]. Preheating was done using gas flame. During the preheating process, temperature was measured through E-type thermocouple. Cladding was done as soon as the preheat temperature was reached with GTAW process. Cladding was carried out in the single pass and the weld metal was cooled in the presence of air. The thickness of the coating was nearly 1-1.5 mm and the GTAW parameters can be seen in Table 2.

Table 2: GTAW parameters

parameter	value
Welding Voltage / V	11
Welding current/ A	120
Welding speed / mm s^{-1}	0.7
Electrode polarity	DCEN
Welding position	Horizontal-flat
Shielding gas	Argon

The welding parameters were selected based on the results obtained in several primary experiments and the data already available in the related literature [18]. After the cladding, the surface of the sample was flattened by grinding for wear test and the microstructure study. The specimen for metallographic examination was sectioned from the clad sample. The cross section of the coating was prepared by sand paper and finally, polished using 0.5µm alumina polishing powder and etched in two etchant solutions. The sample was first etched with 3% nital solution to reveal HAZ and PMZ structure and then etched with a mixture of ethanol, nitric acid and acetic acid in 1:1:1 proportion to reveal the weld metal microstructure. Microstructure observations were done along the vicinity of the centerline of the weld, from the clad layer toward BM, with OLYMPUSE-BX60M OM. Philips Xpert X –ray diffractometer with a Cu Kα monochromated beam (λ = 0.15406 Å) produced at 40 kV and 30 mA was employed to analyse the phase formed in the surface alloyed layer and the interface. The X-ray diffraction was carried out by the step size of 0.05 to scan 2θ from 10° to 100° and the dwell time of 1 second for each step. Metallographic examination was employed to determine the dilution level and measure the individual geometric cross-sectional areas of the deposited filler metal and the melted base metal. The ratio of the melted base metal (A_{bm}) to the total melted cross-sectional area from the filler metal and the base metal ($A_{fm}+A_{bm}$) was regarded as the dilution level[19]:

$$D= A_{bm}/ (A_{fm}+A_{bm}) \quad (1)$$

The software image analyzer (ImageJ) was used to determine the dilution level. The calculated dilution was about 27 % of the total weld volume. In order to determine the chemical composition of the clad layer, optical emission spectroscopy technique was used. The results are shown in table 1.The hardness was measured by means of Vickers Buehler microhardness machine using the applied load of 200 mg and the dwell time of 15 seconds on the transverse cross section of the alloyed layer. The wear resistance of the clad layer and DI was evaluated by the reciprocating pin on the plate machine. The cylindrical pin, 6 mm in diameter and 12 mm in length, with a spherical cap, was used as the counterpart material. Pin material was 52100 bearing steel with an average hardness of 64 HRC (800 HV). The chemical composition of the pin can be seen in table 1.The tests were performed at the constant sliding velocity of 0.21 m/s under the applied load of 60 and 90 N at room temperature. The sample's weight losses after every 100m of the sliding distance up to 1000m were measured using an electronic balance (±0.1 mg). After the wear test, the worn surface and the wear debris of the clad layer and DI were observed in the SEM to determine the predominant wear mechanism.

Results and Discussion

Microstructure

The microstructure of as-weld specimen is shown in Fig. 1. This figure reveals that the welded sample had four distinct regions including the clad layer, the partially melted zone, the heat affected zone and the unaffected base metal. The microstructure of the clad layer can be seen in Fig. 2. It can be observed that the microstructure of the coating consisted of at least two phases, dendritic and interdendritic.

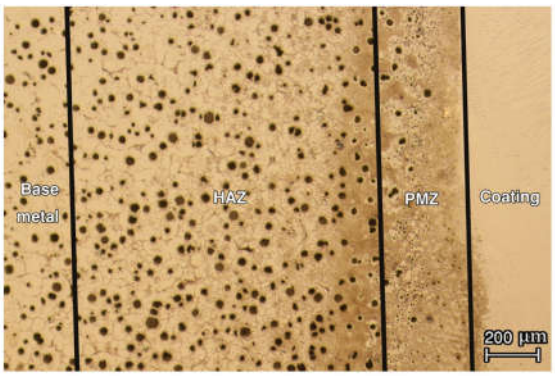

Figure 1: Optical micrograph of the microstructure of as-weld specimen

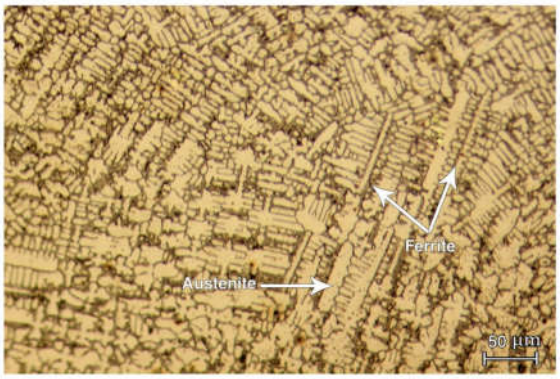

Figure 2: Optical micrograph of the clad layer

To identify the phases existing in duplex stainless steel, the Fe-Cr-Ni ternary diagram can be used. A section of the ternary diagram at 55% Fe (isoplethal section) has been illustrated in Fig. 3. The chemical composition of the alloyed layer has been marked by C_0 in Fig. 3. The ternary diagram shows that ferrite is the primary solidification phase in this alloy. According to the ternary diagram, the outer portions of ferrite dendrites, which are formed in the final stage of solidification, have less Cr than the cores of dendrites, which are formed in the first stage of solidification. During cooling in the two-phase region, austenite is formed at the expense of ferrite. As previously mentioned, the outer portions of the ferrite dendrites have lower Cr and austenite can be formed at this site. Therefore, all the exterior portions of ferrite dendrites are completely transformed to austenite while core parts remain unchanged. Other researchers have reported similar results in GTA welding of 309 stainless steel [20]. In Fig. 2, the dark region and the light region are the remaining ferrite (Cr rich) and austenite, respectively. Because of the complex alloying of the clad layer, a number of precipitation reactions such as carbide and nitride formation could occur below 1000 ˚C. The type of precipitation reaction depends on time and temperature [16]. The XRD pattern of the clad layer illustrated in Fig. 4 can confirm the presence of carbide and nitride phases. Variation in the solidification mode along the cross section of the clad layer is shown in Fig. 5. It can be seen that solidification mode was changed from cellular to columnar

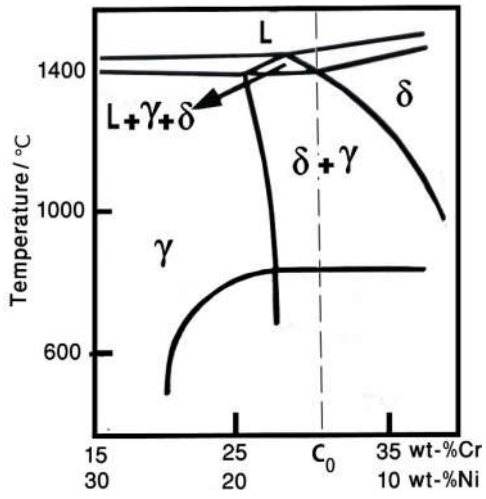

Figure 3: The Fe-Cr-Ni pseudo binary phase diagram at 55%Fe

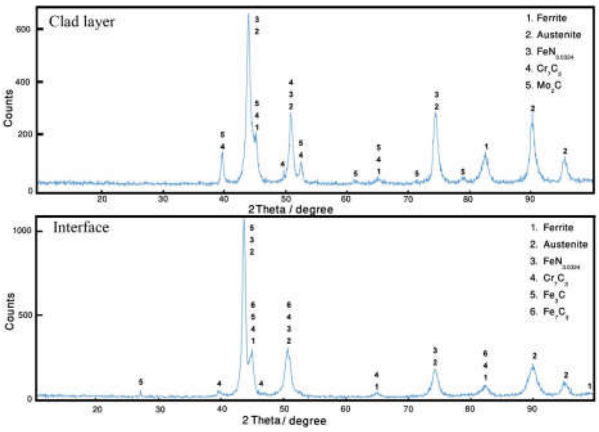

Figure 4: X-ray diffraction pattern of the clad layer and the interface

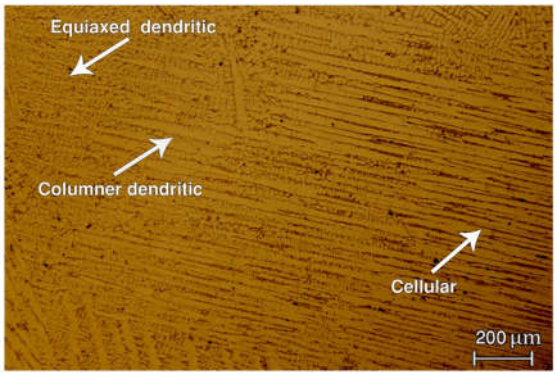

Figure 5:Optical micrograph of transition in the solidification mode

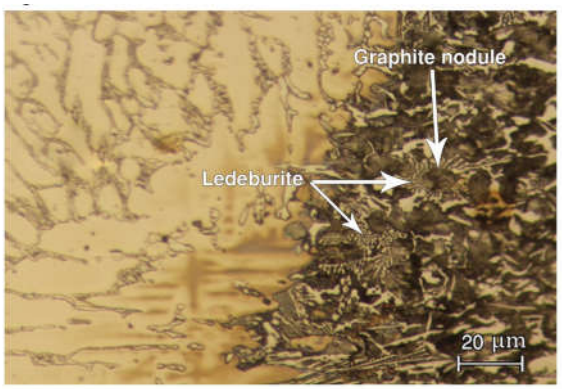

Figure 6: Optical micrograph of Ledeburite formation in PMZ

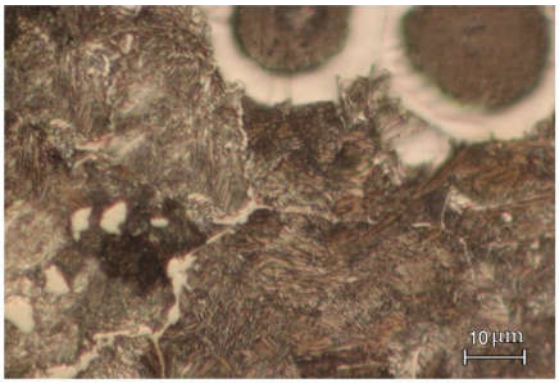

Figure 7: Pearlite microstructure in the HAZ

dendritic and equiaxed dendritic from the substrate toward the clad layer due to the change of G/R ratio (G: temperature gradient/R: solidification rate) during the solidification of the clad layer [20].

The surface of ferritic DI, due to the arc's heat, was in the semi molten condition. Since the solubility of graphite in liquid was more than that in solid, the graphite nodules began to dissolve and so, carbon content of liquid was increased, reaching to the eutectic point in Fe-C binary diagram. The smaller graphite nodules in PMZ, rather than HAZ and BM, as shown in the Fig. 1, confirmed the dissolution of the graphite nodule. Due to the high cooling rate of solidification process, the graphitic iron could not be formed and instead, the liquid was solidified as the white iron. Formation of ledeburite in the PMZ of ductile iron has been reported by other researchers[3, 21]. Since the carbon content of areas near the graphite nodules was higher than that of other regions, the probability of ledeburite formation in these regions was more than the other one. The formation of ledeburite in the vicinity of the graphite nodules can be seen in Fig. 6.

HAZ in the heating cycle reached the eutectoid temperature, thereby transforming to the austenite; so, as can be understood from the Fe-C binary diagram, graphite started to dissolve, thereby increasing the carbon content of the matrix. In the cooling cycle, austenite transformation was expected to occur at the eutectoid temperature. Carbon diffusion could not completely happen because of the relatively high cooling rate; therefore, in the vicinity of graphite nodules, due to the short distance, carbon was diffused and the matrix was transformed to the ferrite and the farther areas were transformed to the pearlite. This microstructure is known as bull's eye structure [22, 23]. Fig. 7 illustrates the HAZ microstructure. The light areas in the vicinity of graphite nodules represent ferrite and the dark regions are pearlite colonies. Also, the results of microhardness confirmed the pearlite formation in the HAZ. El Banna et al. [24] have shown that many factors such as the level of preheating, heat input, type of filler metal and post weld heat treatment can affect the microstructure of HAZ in the welding of DI. Askari et al. [21] have found that preheating is the most important factor affecting HAZ structure in the welding of DI. So pearlite formation in HAZ can be attributed to the preheating of specimen. Also, Ebrahimnia et al. [25], in the cladding of DI with nickel base alloy, have shown that preheating and post heating operations lead to the formation of the coarse pearlite in the HAZ of DI. However, the formation of martensite has been reported by Shamanian et al. [11] in the cladding of ductile iron by austenitic stainless steel electrode, Arabi et al. [10, 12, 13] in the surface alloying of ductile iron through Stellite 6, Inconel 617 and ENiCrFe3 electrodes, Heydarzadeh Sohi et al. [5] in surface melting and chromium surface alloying of ductile iron, Li et al. [26]in laser cladding of ductile iron through Fe-Cr alloy and Abboud [27] in the surface modification of nodular cast iron by GTA welding.

Microhardness

Hardness plays an important role in the wear behaviour of materials [5]. The following equation shows the relationship between hardness and the wear behaviour of the materials[28]:

$$Q=K.W.V/H \qquad (2)$$

where Q is the wear rate, W is the applied load, V is the sliding speed, H is the hardness and K is a constant.

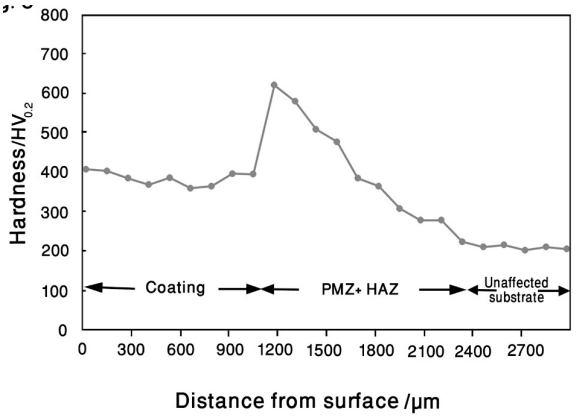

Figure 8: Microhardness profile along the cross section of the surfaced alloyed layer

Thus, according to equation 2, the wear rate is reduced by increasing the hardness. The microhardness profile as a function of distance from the surface is shown in Fig. 8. The hardness of the as received DI was 220 HV. The hardness was approximately uniform along the thickness of the coating with the average value of 390 HV and it was increased to about 620 HV at the interface. The hardness of the interface region was sharply increased in comparison with both alloyed layer and BM. Since the hardness significantly depends on the phases present, the high value of the hardness in the interface region can be related to the presence of many carbides and nitrides formed during solidification and solid transformation [10]. Fig. 4 shows the XRD pattern of the interface region vouching the presence of these hard phases.

Wear test

In order to compare the wear behaviour of the coated sample and DI, the weight loss of two samples as a function of the sliding distance in the wear testis shown in Fig.9. As can be seen, the wear resistance of the coated sample was significantly higher than that of ferritic DI. The better wear behaviour of the coated sample can be related to the higher hardness value of this sample. Furthermore, solidification structure, nature, shape and distribution of the present phases and many other factors such as oxidation films and the strong binding between the matrix and the reinforcement in the composite materials can affect the wear behaviour of the engineering materials [29, 30].

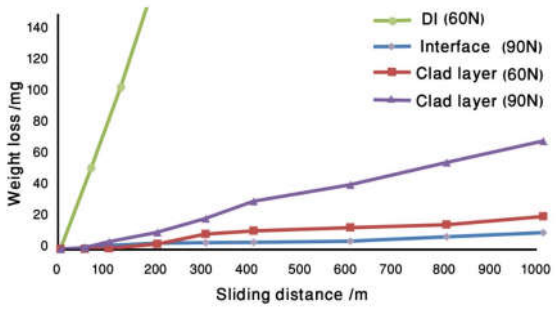

Figure 9: Weight loss as a function of the sliding distance for the substrate, the cladded layer and the interface

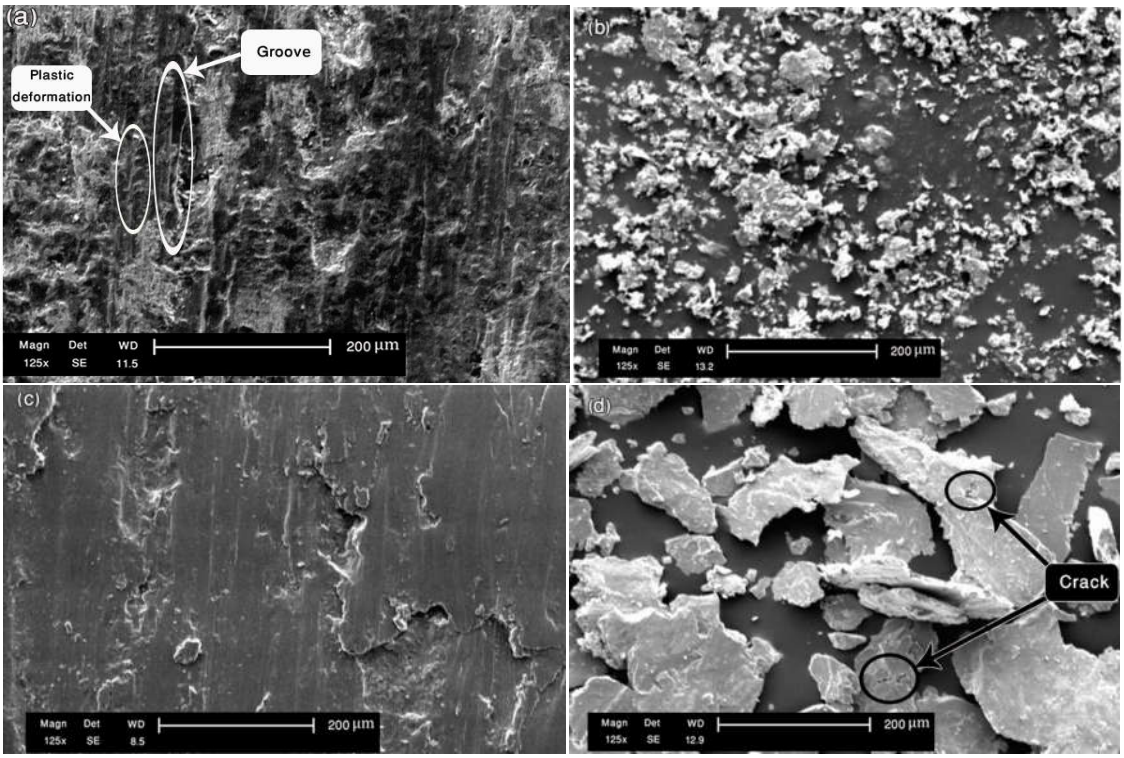

Figure 10: SEM micrograph of: (a) the wear surface of DI, (b) the worn debris of DI, (c) the wear surface of the clad layer and (d) the worn debris of the clad layer

In order to understand the wear life of the coated sample, wear test on interface was performed. Fig.9 also shows the wear resistance of the interface in comparison with the coated sample. The wear rate was 80.6×10^{-3} mg/m and 11×10^{-3} mg/m for the clad layer and the interface, respectively. As can be observed, the wear resistance of interface was about seven times higher than that of the clad layer. So, as time passes, the wear rate is decreased.

The wear mechanisms were characterized by SEM topography of the worn surface and wear debris. The micrographs of the worn surface and the wear debris of the coated and DI specimens are shown in Fig.10a-d.The worn surface of DI (Fig.10a)had deep and clearly long continuous grooves extending parallel to the sliding direction and a large number of plastic deformations, all indicating the abrasive wear [31]. Due to the big difference in the hardness values of substrate and its counterpart, the pin could plow the DI substrate and create the grooves and plastic deformation, as can be observed in Fig.10a. In addition, the abrasive wear could be contributed by work-hardened wear debris.Small and relatively spherical wear debris of DI, as observed in Fig. 10b, could be attributed to the low hardness of this specimen. Wear debris was entrapped between the two sliding surfaces. Due to low hardness, deformation to the spherical shape or breakage in to the small particles (work-hardened wear debris) occurred [13]. Also, the worn surface of DI substrate was very harsh.During the wear test, when the pin (counterpart) was in contact with the surface of DI (sample), the temperature was locally raised at the contact point. So, hardness near this point was quickly decreased, leading to serious plastic deformation, local contact welding between the contacting asperities and materials transfer. Therefore, it was expected that serious material removal from friction surface would occur and very harsh surface could be created [32]. It should be noted that if the shear strength of the contacting region is between those of the two contacting materials, material will be easily transferred from the soft one to the hard one [30].The hardness of the DI (220 HV) was obviously lower than that of the counterpart (800 HV), hence the material transfer was from the soft disk to the hard pin. The weight gain of the pin proved the material transfer form DI disk to the steel pin. Yanet al.[4] and Huang et al. [31] have reported similar results for the wear mechanism of ductile iron and Ti-6Al-4V, respectively. According to Fig.10c, the possible predominant wear mechanism of the coated sample was delamination. It should also be added that evaluation of wear debris can complete the information obtained from wear track. The shape of the wear debris, as shown in Fig. 10d (thin and flake-shape), confirmed that the delamination was the predominant wear mechanism for the coated specimen [13]. Moreover, cracks were observed in the wear debris as shown in Fig.10d. This could be another reason why the predominant wear mechanism was delamination. According to the delamination theory, the shear plastic deformation, crack initiation and its propagation near surfaces can lead to debris lamination [11]. Arabi et al. [12] have also observed delamination mechanism in DI surface alloyed with Ni based electrode.

Conclusions

1. Ferritic-austenitic duplex stainless steel was successfully deposited on the surface of ferritic DI by GTAW process. The clad layer had a dendritic microstructure that consisted of ferrite, austenite, carbides and nitrides.
2. Due to the change of G/R ratio, solidification mode was changed from cellular to columnar dendritic and

Contents lists available at http://www.jmsse.in/ & http://www.jmsse.org/

equiaxed dendritic, from the substrate toward the clad layer.

3. The microstructure of HAZ included pearlite, ferrite and graphite nodules. The pearlite formation in this region could be attributed to the preheating of specimen.
4. Due to the high cooling rate during the solidification process, ledeburite was formed in the PMZ.
5. Wear resistance of DI was significantly improved using duplex stainless as the coating material. The high resistance of the clad layer, rather than DI, could be related to the presence of hard phases such as Mo_2C, Cr_7C_3 and $FeN_{0.0324}$.
6. The wear resistance of the interface was meaningfully higher than that of the clad layer, so the wear rate could be reduced during time.

References

1. E.M. El-Balnna, study of ferritic centrifugally cast ductile cast iron, Mater. Lett. 1994, 20, 99-106.
2. A. Akdemir, M. Tekeli, N. Ataberk, Fatigue crack growth behaviour in ferritic ductile iron with surface crack under reverse bending, J. Comp. Mater. Sci. 2007, 41, 38-43.
3. Q. Xiaoben, Z. Shigen, F. Jinhui, Rolling contact fatigue performance of ductile iron improved by electric contact surface strengthening, J. Tribol. Int. 2013, 60, 58-63.
4. Y. Hua, W. Aihua, X. Zhaoting, X. Kaidong, H. Zaowen, Microstructure and wear resistance of composite layers on a ductile iron with multicarbide by laser surface alloying, Appl. Surf. Sci. 2010, 256, 7001-7009.
5. M. HeydarzadehSohi, M. Ebrahimi, H.M. Ghasemi, A. Shahripour, Microstructural study of surface melted and chromium surface alloyed ductile iron, Appl. Surf. Sci. 2012, 258, 7348-7353.
6. N. Venkateswara Rao, G. Madhusudhan Reddy, S. Nagarjuna, Weld overlay cladding of high strength low alloy steel with austenitic stainless steel Structure and properties, Mater. Des. 2011, 32, 2496-506.
7. F. Madadi, M. Shamanian, F. Ashrafizadeh, Effect of pulse current on microstructure and wear resistance of Stellite6/tungsten carbide claddings produced by tungsten inert gas process, Surf. Coat. Technol. 2011, 205, 4320-4328.
8. D.L. Olson, T.A. Siewart, S. Liu, G.R Edwards, ASM Handbook, Vol. 6 Welding, Brazing and Soldering, ASM International, Ohio, 1993.
9. F. Madadi, F. Ashrafizadeh, M. Shamanian, Optimization of pulsed TIG cladding process of stellite alloy on carbon steel using RSM,J. Alloys Compd. 2012, 510, 71-77.
10. R. ArabiJeshvaghani, M. Jaberzadeh, M. Zohdi, M. Shamanian, Microstructural study and wear behavior of ductile iron surface alloyed by Inconel 617, Mater. Des. 2014, 54, 491-497.
11. M. Shamanian, S.M.R. Mousavi Abarghouie, S.R. Mousavi Pour, Effects of surface alloying on microstructure and wear behavior of ductile iron, Mater. Des. 2010, 31, 2760-2766.
12. R. ArabiJeshvaghani, E. Harati, M. Shamanian, Effects of surface alloying on microstructure and wear behavior of ductile iron surface-modified with a nickel-based alloy using shielded metal arc welding, Mater. Des. 2011, 32, 1531-1536.
13. R. ArabiJeshvaghani, M. Shamanian, M. Jaberzadeh, Enhancement of wear resistance of ductile iron surface alloyed by stellite 6, Mater. Des. 2011, 32, 2028-2033.
14. A. Amirsadeghi, M. HeydarzadehSohi, Comparison of the influence of molybdenum and chromium TIG surface alloying on the microstructure, hardness and wear resistance of ADI, J. Mater. Process. Technol. 2008, 201, 673-677.
15. G. Sun, R. Zhou, P. Li, A. Feng, Y. Zhang, Laser surface alloying of C-B-W-Cr powders on nodular cast iron, Surf. Coat. Technol. 2011, 205, 2747-2754.
16. J.C. Lippold, D.J. Kotecki, Welding metallurgy and weldability of stainless steels, John Wiley & Sons, New Jersey, 2005.
17. G. Chali, P. Kangas, Super and hyper duplex stainless steels: structures, properties and Application, Procedia Struct. Integrity. 2016, 2, 1755-1762.
18. A.Mourad, A. Khourshid, T. Sharef, Gas tungsten arc and laser beam welding processes effects on duplex stainless steel 2205 properties, Mater. Sci. Eng. A. 2012, 549, 105-113.
19. Y.L. Suna, G. Obasib, C.J. Hamelinc, A.N. Vasileioua, T.F. Flinta, J. Balakrishnana, M.C. Smitha, J.A. Francis, Effects of dilution on alloy content and microstructure in multi-pass steelWelds,mater. process. Technol. 2019, 256, 71-86.
20. S. Kou, Welding metallurgy, John Wiley, New Jersey, 2003, Ed. 2.
21. M. AskariPaykani, M. Shayan, M. Shamanian, Weldability of ferritic ductile cast iron using full factorial design of experiment, J. Iron Steel Res. Int. 2014, 21, 252-63.
22. A. Zammit, S. Abela, J.C. Betts, M. Grech, Discrete laser spot hardening of austempered ductile iron, Surf. Coat. Technol. 2017, 331, 143-152.
23. D.M. Stefanescu, ASM Handbook, Vol. 15, Casting, ASM International, Ohio, 1988.
24. E.M. El-Banna, M.S. Nageda, M.M. Abo El Saadat, Study of restoration by welding of pearlitic ductile cast iron, Mater. Lett. 2000, 42, 311-320.
25. M. Ebrahimnia, F. MalekGhaini, S. Gholizade, M. Salari, Effect of cooling rate and powder characteristics on the soundness of heat affected zone in powder welding of ductile cast iron, Mater. Des. 2012, 33, 551-556.
26. Y. Li, Sh. Dong, Sh. Yan, X. Liu, P. He, P. Xu, Microstructure evolution during laser cladding Fe-Cr alloy coatings on ductile cast iron, Opt. laser. Thecnol. 2018, 108, 255-264.
27. J. HadiAbboud, Microstructure and erosion characteristic of nodular cast iron surface modified by tungsten inert gas, Mater. Des. 2012, 35, 677-684.
28. P.J. Blau, ASM handbook, Vol. 18, Friction, lubrication, and wear technology, ASM International, Ohio, 1992.
29. Y.C. Lin, Y.C. Chen, Reinforcements affect mechanical properties and wear behavior of WC clad layer by gas tungsten arc welding, Mater. Des. 2013, 45, 6-14.
30. H. Yan, P. Zhang, Z. Yu, Q. Lu, S. Yang, C. Li, Microstructure and tribological properties of laser-clad Ni–Cr/TiB2 composite coatings on copper with the addition of CaF2, Surf. Coat. Technol. 2012, 206, 4046-4053.
31. C. Huang, Y. Zhang, R. Vilar, J. Shen,Dry sliding wear behavior of laser clad TiVCrAlSi high entropy alloy coatingson Ti–6Al–4V substrate, Mater. Des. 2012, 41, 338-343.
32. X. Wang, M. Zhang, X. Liu, S. Qu, Z. Zou,Microstructure and wear properties of TiC/FeCrBSi surface compositecoating prepared by laser cladding, Surf. Coat. Technol. 2008, 202, 3600-3606.